Dynamic solidification of a binary melt

Herbert E. Huppert* **& M. Grae Worster†**

* Department of Applied Mathematics and Theoretical Physics, University of Cambridge, Silver Street, Cambridge CB3 9EW, UK
† Department of Mathematics, Massachusetts Institute of Technology, Cambridge, Massachusetts 02139, USA

The fundamental physics and fluid dynamics of a solidifying two-component system cooled from below is analysed quantitatively. Theoretical results for the rate of growth of the solid are in good agreement with experimental measurements on crystallizing aqueous solutions. The results are applicable to the solidification of a wide variety of binary alloys.

THE cooling and resultant solidification of a melt is important in many different fields, including crystal growth[1,2], electrical engineering[3,4], geology[5,6], geophysics[7,8], metallurgy[9,10] and oceanography[11,12]. The investigation of the fluid dynamic processes which often dominate solidification has been advanced by the suggestion[13-15] that the mechanisms may be elucidated by laboratory experiments on the freezing of aqueous solutions. In some cases[14,15] the studies were aided greatly by the concurrent analysis of a predictive mathematical model. Here, we use this powerful approach and describe some simple experimental and associated theoretical models for the cooling and crystallizing at a horizontal boundary of an initially homogenous fluid. The aim is to highlight the fundamental phenomena and to minimize consideration of inessential details by studying a simple and straightforward situation. We use aqueous solutions because they are easy to handle in the laboratory, but the concepts developed are applicable directly to the solidification of a wide variety of binary alloys.

First, we discuss briefly the phase diagram of the solid/melt mixture and then concentrate on effects associated with cooling and solidifying a melt from below. We determine theoretically the rate of solidification if the solid/melt interface is perfectly flat and horizontal, and also evaluate the criterion for which the interface becomes unstable. In a series of laboratory experiments, we have grown ice with unstable interfaces from different aqueous solutions and we have developed a simple theoretical model whose predictions are in good agreement with the observations. Our main quantitative conclusions are theoretical and experimental relationships for the rate of growth of the crystal block, the total volume of solid produced and an expression for the volume fraction of the solid product.

Phase diagram

The chemical composition of the phase obtained by the solidification of a melt with two chemical components is determined at thermodynamic equilibrium by the phase diagram (Fig. 1). This diagram represents the chemical compositions of melt and solid in equilibrium with each other by the liquidus and solidus respectively. At a temperature and composition represented by a point above the liquidus, the system is liquid. Between the liquidus and the eutectic line, the solidus defines the composition of the material solidifying from the melt, and in general specifies solid phases whose composition differs from both the melt and the pure components of the system[6,9]. For most aqueous solutions and many binary alloys, however, the phase diagram has the special form illustrated in Fig. 1*a*, where solidification from a melt (solution) with sub-eutectic composition yields a solid phase consisting of a pure component (ice). It is usually the case that density in the melt is a much stronger function of composition than of temperature (see Fig. 1), which plays an important role in the fluid dynamics of solidification.

The solidification of a melt of eutectic composition, yielding solid of the same bulk composition, is equivalent to the solidification of a pure material. Otherwise, study of the process of solidification requires that melts with compositions greater and less than that of the eutectic must be dealt with separately, while the direction of cooling (from above or below) also requires distinctive treatment. Table 1 shows the 3×2 matrix by which the problems of solidification may be classified. What follows concentrates mainly on cooling from below of a melt whose composition is below the eutectic value.

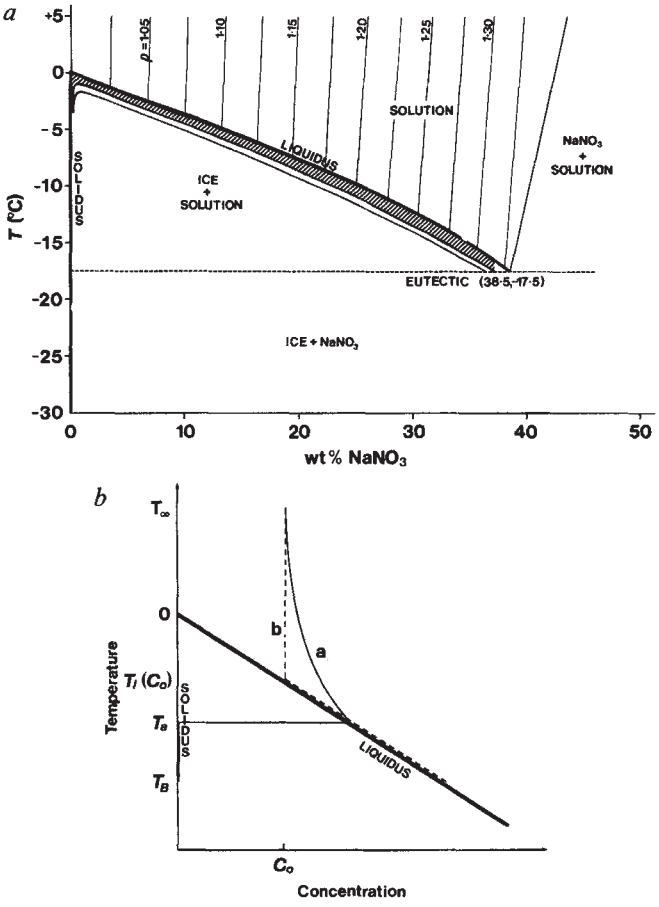

Fig. 1 *a*, Phase diagram for an aqueous solution of $NaNO_3$ (refs 20, 24) with axes of temperature and concentration. The same diagram acts as a schematic for a general binary alloy with components A and B. The figure also presents the lines of constant density with the density values attached. Hatched region, morphologically stable region for $T_\infty = 15$ °C. The curve just beneath the hatched region indicates the curve of marginal stability for $T_\infty = 30$ °C. In determining the curves the following values of the constant physical parameters have been used: $C_{p_m} = 1.0$ cal g^{-1} °C^{-1}, $C_{p_s} = 0.48$ cal g^{-1} °C^{-1}, $D = 10^{-5}$ cm^2 s^{-1}, $L = 80$ cal g^{-1}, $\kappa_m = 0.0013$ cm^2 s^{-1}, $\kappa_s = 0.012$ cm^2 s^{-1}, $\rho_s = 0.916$ g cm^{-3}. Further, the values of Γ and ρ_m were obtained as a function of C_0 from ref. 20. *b*, Phase diagram used here, with temperature and concentration axes chosen so that a solid of zero concentration forms at zero temperature. Heavy solid line, straight-line approximation to the liquidius. Thin curve a, temperature against concentration profile in the morphologically stable regime. Dashed curve b, approximate profile used in our model of the morphologically unstable regime.

Table 1 The six different cases that arise when an initially homogeneous solution is cooled at a horizontal boundary

	Cool from Above	Cool from Below	
$C > C_E$	13	25	Light fluid released
$C = C_E$	13	14	Uniform composition throughout
$C < C_E$	22	here	Heavy fluid released
	Thermally unstable	Thermally stable	

Numbers refer to the reference in which each case is discussed. See text for explanation of symbols.

Eutectic growth

The solidification of a melt of eutectic composition involves only variations in temperature, because the composition in the melt and solid is constrained to remain at the eutectic value. This situation is equivalent to one described by Carslaw and Jaeger[16], who present the analytical solution for a column of melt of infinite height whose initial temperature is T_∞ and which is cooled at a lower boundary whose temperature is T_B. We conducted two experiments using eutectic compositions of aqueous Na_2CO_3 (eutectic composition $C_E = 5.7$ wt%, eutectic temperature $T_E = -2.1$ °C) in an insulated Perspex tank 20 cm × 20 cm × 45 cm high. Our observations of the height of the compact eutectic solid as a function of time in one of our experiments are plotted in Fig. 2. They are in good agreement with the analytical solution, which attests to the reliability of our experimental methods.

Sub-eutectic growth

We have extended the study of the solidification of a eutectic melt to the case where the composition is not that of the eutectic but in which the initial uniform concentration of solute C_0 is less than C_E. Solid of composition $C = 0$ grows on the cooled boundary and, to begin with, we assume that the solid/melt interface remains flat and parallel to the boundary. The fluid released by the crystallization is relatively heavy and thus remains just above the interface, so that the concentration gradient which develops is stable. Thus, no physical motion takes place and the transport of heat and solute is by molecular diffusion alone. The governing equations are then those for heat transport (in one dimension, taken as z measured upwards from the cooled boundary) above and below the interface and for solute diffusion in the melt. The equations for the temperature $T(z, t)$ and the composition $C(z, t)$ are

$$\rho_s C_{p_s} \frac{\partial T}{\partial t} = k_s \frac{\partial^2 T}{\partial z^2} \quad \text{(for } z < h(t), \text{ the position of the moving boundary)} \tag{1}$$

$$\left.\begin{aligned} \rho_m C_{p_m} \frac{\partial T}{\partial t} &= k_m \frac{\partial^2 T}{\partial z^2} \qquad (2)\\ \frac{\partial C}{\partial t} &= DL \frac{\partial^2 C}{\partial z^2} \qquad (3)\end{aligned}\right\} (z > h(t); \text{ that is, for } z \text{ in the melt})$$

$$T = T_B \qquad (z = 0) \tag{4}$$

$$T \to T_\infty, \; C \to C_0 \qquad (z \to \infty \text{ or } t \to 0) \tag{5}$$

The physical parameters are the solute diffusivity D, the thermal conductivity k, the density ρ and the specific heat C_p, all of which are considered to be constant. Subscripts s and m refer to properties of the solid and the melt, respectively. The difference in heat flux across the interface $z = h(t)$ results from the latent heat released on solidification. This can be expressed by

$$\rho_s L\dot{h} = -k_m \frac{\partial T}{\partial z}(h+, t) + k_s \frac{\partial T}{\partial z}(h-, t) \tag{6}$$

where a dot denotes a time derivative and L is the latent heat of fusion. Conservation of solute requires

$$C(h+, t)\dot{h} = -D \frac{\partial C}{\partial z}(h+, t) \tag{7}$$

Further, with the assumption that the solidification kinetics can be described by equilibrium thermodynamics, we require that the temperature and composition at the interface lie on the liquidus, which we approximate by the linear relationship

$$T = T_L(C) = -\Gamma C \tag{8}$$

This tacitly assumes, merely for convenience, that the liquidus temperature is 0 at zero composition, as it is for all aqueous solutions.

The system of equations and boundary conditions represented by equations (1)-(8) admits a similarity solution, with variable

$$\eta = \tfrac{1}{2}(Dt)^{-1/2} z \tag{9}$$

in which the interface has position

$$h = 2\lambda(Dt)^{1/2} \equiv \gamma_C^{t^{1/2}} \tag{10, 10'}$$

This similarity form of solution can be shown to be the only solution of the equations. The temperature and concentration fields, determined from equations (1)-(5), can then be expressed in terms of error functions[17] as

$$T(z, t) = T_B + (T_a - T_B)\,\mathrm{erf}\,(\varepsilon_s \eta)/\mathrm{erf}\,(\varepsilon_s \lambda) \qquad (z < h) \tag{11}$$

$$\left.\begin{aligned} T(z, t) &= T_\infty + (T_a - T_\infty)\frac{\mathrm{erfc}\,(\varepsilon_m \eta)}{\mathrm{erfc}\,(\varepsilon_m \lambda)} \qquad (12)\\ C(z, t) &= C_0 + (C_a - C_0)\frac{\mathrm{erfc}\,\eta}{\mathrm{erfc}\,\lambda} \qquad (13)\end{aligned}\right\} (z > h)$$

where T_a and C_a are the temperature and concentration of the melt at the interface. There are two parameters $\varepsilon_{s,m} = (D/\kappa_{s,m})^{1/2}$, where $\kappa = k/\rho C_p$ is the thermal diffusivity. The interface conditions in equations (6)-(8) are now used to determine the eigenvalue λ from

$$\Gamma C_0 \left[\frac{F(\lambda)}{1 - F(\lambda)}\right]\left[\frac{\rho_m C_{p_m}}{F(\varepsilon_m \lambda)} + \frac{\rho_s C_{p_s}}{G(\varepsilon_s \lambda)}\right] = \frac{\rho_s C_{p_s} T_1}{G(\varepsilon_s \lambda)} - \frac{\rho_m C_{p_m} T_0}{F(\varepsilon_m \lambda)} - \rho_s L \tag{14}$$

where

$$F(x) = \pi^{1/2} x e^{x^2}\,\mathrm{erfc}\,x, \qquad G(x) = \pi^{1/2} x e^{x^2}\,\mathrm{erf}\,x$$

$$T_1 = T_L(C_0) - T_B, \qquad T_0 = T_\infty - T_L(C_0)$$

The solute diffusivity D is typically much smaller than the thermal diffusivity κ. In this case, $\varepsilon \ll 1$, and in the limit $\varepsilon \to 0$ equation (14) reduces to the simpler expression

$$F(\lambda) \approx [1 + (\Gamma C_0/T_1)]^{-1} = (C_a - C_0)/C_0 \tag{15, 15'}$$

Because F increases monotonically from 0 to 1, equation (15) has a unique solution of λ of order unity. This confirms the scaling used in equation (10) and indicates that the growth of the flat interface is controlled by solute diffusion. Note, however, that when C_0 is small (of the order of $\varepsilon^2 = D/\kappa$, with κ_s/κ_m of the order of unity) the growth is no longer controlled by solute diffusion but rather by thermal diffusion. This is indicated by the fact that in this event $\lambda = O(\varepsilon^{-1})$ and so $h = O(\kappa t)^{1/2}$. It would be interesting to carry out an experimental verification of the validity of equation (14).

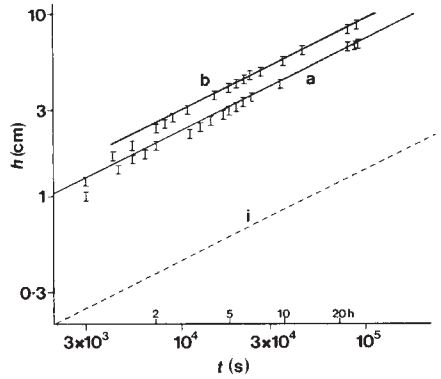

Fig. 2 Experimental and theoretical data on the height of the block as a function of time. Line a, an experiment using a Na_2CO_3 solution at eutectic composition with $T_B = -5.7$ °C, $T_\infty = 17.3$ °C. Line b is the representative experiment R with parameters in the morphologically unstable regime. Line b is the prediction of the theoretical model whereas line i is the predicted height of a flat interface at the same conditions.

Morphological instability

If the undercooling, $T_L - T_B$, is too large, solidification proceeds too quickly and the solidification interface is no longer planar. It grows in a spatially irregular manner, which will be described photographically in more detail below. The initial break-up of the planar interface is often called morphological instability. A useful physical description of the instability is discussed at length by Langer[18]. Detailed calculations[19] indicate that, on the assumption that surface tension effects are negligible, instability occurs when

$$k_s \frac{\partial T}{\partial z}(h-, t) + k_m \frac{\partial T}{\partial z}(h+, t) = -(k_s + k_m)\Gamma \frac{\partial C}{\partial z}(h+, t) \quad (16)$$

If thermal conductivity in the solid is neglected ($k_s = 0$), equation (16) becomes equivalent to the statement that instability arises whenever the predicted values of temperature and composition on the melt side of the interface lie beneath the liquidus (where the system should be partially solid). The diffusion of heat in the solid away from the interface somewhat alters the onset of instability. Surface tension does not alter equation (16) significantly in most practical situations, so we may use it as a good approximate criterion and express it in terms of our similarity solution as

$$T_0 < \Gamma C_0 \left[\frac{F(\lambda)}{1 - F(\lambda)}\right]\left[\frac{k_m + k_s}{2k_m}\frac{F(\varepsilon_m \lambda)}{\varepsilon_m^2 F(\lambda)} - 1\right] - \frac{1}{2}\frac{\rho_s}{\rho_m}\frac{L}{C_{p_m}} F(\varepsilon_m \lambda) \quad (17)$$

For given values of T_∞ and C_0 the value of T_B at which supercooling first occurs is found by solving equation (17) simultaneously with equation (14). The critical value of T_B is plotted as a function of C_0 for two values of T_∞ in Fig. 1*a*.

Experiments

We performed 12 experiments with various solutes at different values of T_B and C_0 in the tank described above. Temperatures were monitored continuously with thermistors, some of which were held fixed, and the ice block allowed to freeze around them. Occasional measurements of concentration were made by withdrawing small samples and analysing them with a hand-held refractometer. All the experiments were in the morphologically unstable regime.

The results of a representative experiment, denoted by R ($NaNO_3$; $T_B = -16.5$ °C, $T_\infty = 14.7$ °C and $C_0 = 14$ wt%), are shown in Figs 2–4. Figure 3 shows three views of the solid ice block after it was removed from the tank. The humpy form of the surface (Fig. 3*a*) and the small-scale facets (Fig. 3*c*) depict cearly that the system is in the morphologically unstable regime. Figure 2 presents the (maximum) height of the block as a function of time and compares this with the result obtained by solving equations (10) and (14). The difference between the two indicates that the contortions of a morphologically unstable surface allows it to grow much more rapidly than if it were to remain stable. Figure 4 presents experimental and theoretical data on temperature and concentration at various times. There is considerble difference between the experimental results and those given by equations (11)–(14). The generality of this disagreement is confirmed in Fig. 5 which compares the experimental values of γ with those given by equations (11)–(14) for varying initial C_0 at fixed T_B and varying T_i at fixed C_0.

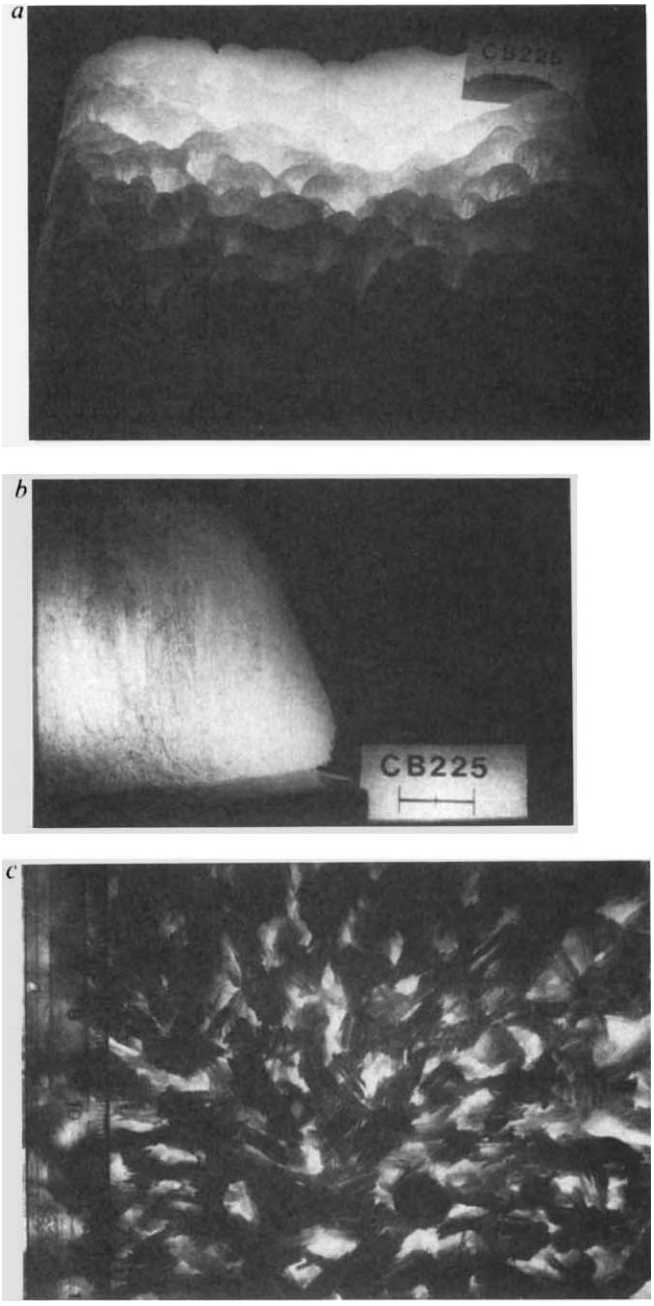

Fig. 3 *a*, An oblique view of the top of the ice block in experiment R showing the humpiness of the surface on a scale of centimetres and the finer scale 'facets' on a scale <1 mm. Horizontal scale, 2 cm long. *b*, Vertical view of the same experiment showing the lines of solid ice and the compositionally-enriched fluid. *c*, Close-up view looking vertically downwards onto the top of the block in the same experiment. Note the very fine-scale irregularities.

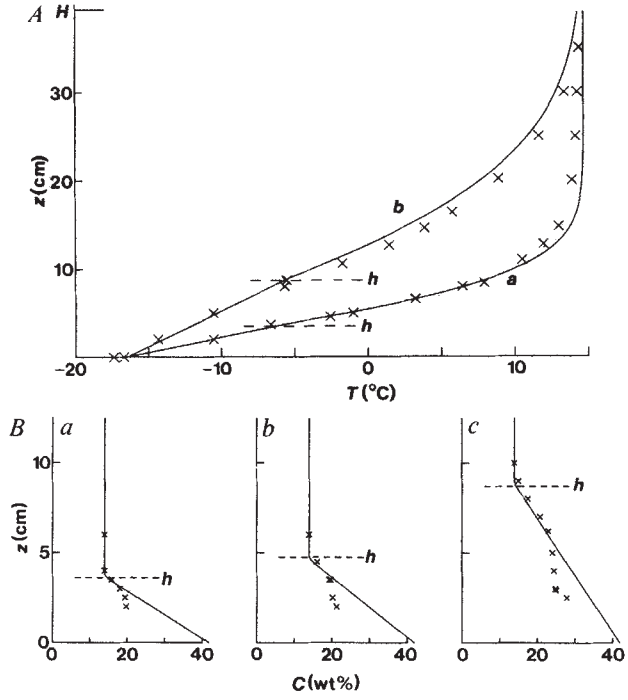

Fig. 4 *A*, Temperature profiles as a function of depth for experiment R at *a*, 3 h 40 min and *b*, 25 h 35 min. Crosses, data points; dashed lines, observed heights, *h*, of the ice block. Solid curves, temperatures predicted by the model of the mush. *B*, Composition profiles as a function of depth for experiment R at *a*, 3 h 20 min; *b*, 7 h 0 min; *c*, 25 h 20 min. Crosses, $NaNO_3$ concentration in fluid withdrawn by means of inserting a thin sampling tube; dashed lines, observed heights, *h*, of the ice block; solid curves, concentrations predicted by the model of the mush.

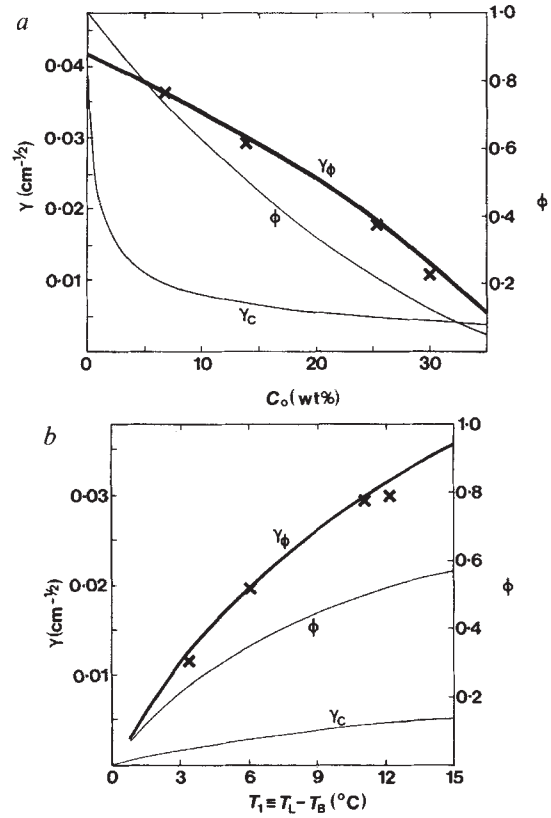

Fig. 5 *a*, Growth rate coefficient (γ) and solid fraction (ϕ) as functions of concentration for $T_B = -17$ °C and $T_\infty = 15$ °C. The crosses are experimental values of λ. The heavy curve is the theoretical prediction obtained by solving equations (22) and (23). The light curve γ_C is the result of the model which assumes a flat interface and results in equation (14). *b*, γ and ϕ as a function of the undercooling $T_1 = T_L - T_B$ for $C_0 = 14$ wt% and $T_\infty = 15$ °C.

Theoretical model

The experimental observations described here suggest that a mixed phase of solid and melt, sometimes called a mush phase, is formed when the flat interface is morphologically unstable. Equations describing the evolution of a mush have been developed previously[21,22] and similarity solutions have been found[21]. These equations relate bulk properties of the mush, averaged over a length scale larger than the typical crystal spacing. Thus, when a melt is cooled from below and crystallizes in such a way that relatively heavy fluid is released, the averaged equations predict convective stability of the interstitial fluid. The large pore size in the ice-blocks, however, suggested that compositional convection resulting in solute redistribution had occurred on a sub-pore scale. This would render the previous models inapplicable to the present situation. However, a simple predictive model of the growth of the mush (when $T_B > T_E$) can be developed, based on the controlling nature of thermal diffusion and the appropriate use of bulk conservation relationships.

We assume, for simplicity, that the densities of the solid and melt are the same. The mush extends from the cooled boundary to some position $z = h(t)$ and we assume the solid fraction, ϕ, within the mush to be constant. In reality, ϕ varies with height, but our model conserves mass only on a global scale and the constancy of ϕ is a necessary and consistent approximation. The solute concentration has uniform value C_0 throughout the melt in $z > h$ and obeys the liquidus relation described by equation (8) in the interstices of the mush. Diffusion governs the heat transfer in both the mush and the melt. Thus the thermal field is given by equations (11) and (12) with k_s and C_{p_s} replaced by the approximate expressions, whose validity are discussed by Batchelor[23]

$$\bar{k} = \phi k_s + (1-\phi)k_m \tag{18}$$

and

$$\bar{C}_p = \phi C_{p_s} + (1-\phi)C_{p_m} \tag{19}$$

and T_a replaced by $T_L(C_0)$. Global conservation of solute requires that

$$(1-\phi)\int_0^{h(t)} C\,dz = -\Gamma^{-1}(1-\phi)\int_0^{h(t)} T\,dz = h(t)C_0 \tag{20}$$

while conservation of heat at the mush/melt interface is expressed by

$$\rho L\phi\dot{h} = -k_m\frac{\partial T}{\partial z}(h+,t) + \bar{k}\frac{\partial T}{\partial z}(h-,t) \tag{21}$$

Expressions (11) and (12) are used in equations (20) and (21) to obtain

$$\phi = \left[1 + \frac{\Gamma C_0}{T_1}H(\bar{\delta}\mu)\right]^{-1} \tag{22}$$

$$L\phi = \frac{-C_{p_m}T_0}{F(\mu)} + \frac{\bar{C}_p T_1}{G(\bar{\delta}\mu)} \tag{23}$$

where

$$H(x) = [\exp(x^2) - 1]^{-1}G(x)$$

$$\bar{\delta} = (\kappa_m \rho \bar{C}_p/\bar{k})^{1/2}$$

and

$$\mu = \varepsilon_m \lambda$$

In terms of the new variable μ, the height of the block is given by

$$h = 2\mu(\kappa_m t)^{1/2} = \gamma_\phi t^{1/2} \tag{24, 24'}$$

which confirms that the growth of the block is governed by thermal diffusion. Note, alternatively, that solute diffusion is ignored in the model and correspondingly D does not appear in equations (22), (23) or (24).

Equations (22) and (23) can be solved simultaneously for ϕ and μ. The growth rate coefficient γ_ϕ is plotted as a function of C_0 for fixed T_B in Fig. 5*a* and as a function of T_B for fixed C_0 in Fig. 5*b*. The predicted growth rate is compared with the experimental results in Figs 2 and 5 and the agreement is good.

The measured temperature profiles at two different times during experiment R compare well with the predicted temperatures (Fig. 4*A*) and the measured concentration profiles agree reasonably well (Fig. 4*B*). The disagreement between the experimental data and the theoretical model at points deep in the block may result from the difficulty of inserting a sampling tube reliably to that depth and withdrawing fluid for the concentration measurement.

The validity of the theoretical relationships was tested further by conducting some experiments with different aqueous solutions. The experimental results obtained from using NaCl and NH_4Cl, which have different liquidus relationships and diffusion coefficients, again showed good agreement with the results of the theoretical model.

In conclusion, the experiments and related theory indicate that accurate predictions can be obtained from the use of simple conservation relationships when a melt whose composition is less than the eutectic is cooled from below. Variations of this same approach allow all six different cases, as mapped out in Table 1, to be solved. We plan to publish further details elsewhere.

We thank M. A. Hallworth for technical assistance and J. M. Wheeler, who helped with numerical calculations. We also thank D. R. Fearn, M. C. Flemings, E. J. Hinch, D. T. J. Hurle, R. C. Kerr, J. Lister, D. E. Loper and D. P. McKenzie for critical reading of the manuscript. The research was supported by grants from the BP Venture Research Unit and NERC. The paper was written while the authors were staff members at the 1984 WHOI Geophysical Fluid Dynamics Summer School, which operates under a NSF grant.

Received 3 December 1984; accepted 31 January 1985.

1. Brice, J. C. *The Growth of Crystals from Liquid* (North-Holland, Amsterdam, 1973).
2. Bardsley, W., Hurle, D. T. J. & Mullin, T. B. *Crystal Growth: a Tutorial Approach* (North-Holland, Amsterdam, 1979).
3. Laudise, R. A. *The Growth of Single Crystals* (Prentice-Hall, New York, 1972).
4. Rosenberger, F. *Fundamentals of Crystal Growth* Vol. 1 (Springer, Berlin, 1979).
5. Huppert, H. E. & Sparks, R. S. J. *A. Rev. Earth planet. Sci.* **12**, 11-37 (1984).
6. Ehlers, E. G. *The Interpretation of Geological Phase Diagrams* (Freeman, San Francisco, 1972).
7. Gubbins, D., Masters, T. G. & Jacobs, J. A. *Geophys. J. R. astr. Soc.* **59**, 57-99 (1979).
8. Loper, D. E. & Roberts, P. H. in *Stellar and Planetary Magnetism* (ed. Soward, A. M.) 297-327 (Gordon & Breach, London, 1983).
9. Flemings, M. C. *Solidification Processing* (McGraw-Hill, New York, 1974).
10. Chalmers, B. *Principles of Solidification* (Wiley, New York, 1964).
11. Hobbs, P. V. Ice Physics (Clarendon, Oxford, 1974).
12. Fletcher, N. H. *The Chemical Physics of Ice* (Cambridge University Press, 1970).
13. Chen, C. F. & Turner, J. S. *J. geophys. Res.* **85**, 2573-2593 (1980).
14. Huppert, H. E. & Turner, J. S. *Earth planet. Sci. Lett.* **54**, 144-152 (1981).
15. Turner, J. S., Huppert, H. E. & Sparks, R. S. J. *J. Petrol.* (in the press).
16. Carslaw, H. S. & Jaeger, J. C. *Conduction of Heat in Solids* (Oxford University Press, 1959).
17. Abramowitz, M. & Stegun, I. A. *Handbook of Mathematical Functions* (US Government Printing Office, Washington, 1964).
18. Langer, J. S. *Rev. mod. Phys.* **52**, 1-28 (1980).
19. Sekerka, R. F. *Crystal growth: an Introduction* (ed. Hartman, P.) 403-442 (North-Holland, Amsterdam, 1973).
20. Weast, R. C. (ed.) *Handbook of Chemistry and Physics* (CRC, Cleveland, 1971).
21. Worster, M. G. thesis, Univ. Cambridge (1983).
22. Hills, R. N., Loper, D. E. & Roberts, P. H. *Q. Jl Mech. appl. Math.* **36**, 505-539 (1983).
23. Batchelor, G. K. *A. Rev. Fluid Mech.* **6**, 227-255 (1974).
24. Washburn, E. W. (ed.) *International Critical Tables* (McGraw-Hill, New York, 1929).
25. Kerr, R. C. thesis, Univ. Cambridge (1984).
26. Weeks, W. F. & Ackley, S. F. *Cold Regions Res. Engng Lab. Mon.* 82-1 (1982).

Cordilleria, a newly defined Canadian microcontinent

V. E. Chamberlain & R. St J. Lambert

Department of Geology, The University of Alberta, Edmonton, Alberta, Canada T6G 2E3

Palaeomagnetic data and geological field evidence indicate that most of the western Canadian cordillera lay 1,500 km south of its present position in the early Cretaceous. We suggest that this region comprised a microcontinent, termed Cordilleria, which moved on the Kula plate and collided with the craton ~100 Myr ago to form first the Mackenzie Mountains and then the Rockies.

MODELS for the evolution of the North American cordillera have proliferated since the first attempt[1] at a plate-tectonic synthesis for western North America, based on the classical fivefold division of the cordillera in British Columbia. Earlier models concentrated on the history of palaeosubduction zones; later a long list of dextral transcurrent faults of regional significance were added[2,3] and integration of the United States and Canadian portions of the jigsaw attempted[3,4]. More than 50 microplates and terranes are now recognized[5]. Palaeontological[5-10] and palaeomagnetic (refs 11-16 and E. Irving, G. J. Woodsworth and P. J. Wynne, manuscript in preparation) data clearly show the necessity for major Mesozoic transcurrent movement.

The earlier palaeomagnetic data[11-13] indicated that elements of superterrane Terrane II (ref. 17; Fig. 1) were far travelled. More recent data (refs 14, 15 and E. Irving *et al.*, in preparation) show that Quesnellia and Stikinia, elements of Terrane I (ref. 17), are also far travelled, consistent with the palaeontological evidence[7,8]. The most recent palaeomagnetic evidence (refs 15, 16 and E. Irving *et al.*, in preparation) suggests that both Terranes I and II have been displaced northwards by 14-20° of latitude and rotated clockwise through 45-50° with respect to the North American craton since the early to mid-Cretaceous. These data, from two laboratories and a wide range of Triassic, Jurassic and Cretaceous rocks, show that the southern half of British Columbia was at the present-day relative latitude of California in the early Jurassic, and was probably still there in the early to mid-Cretaceous. The movement to be accommodated between Terranes I and II and the North American craton is ~1,500 km since the mid-Cretaceous. The locus of a possible innermost (eastern) transcurrent fault on which to take up this movement has remained a problem[3,17]. Recent palaeomagnetic evidence is difficult to reconcile with the relatively small geologically observable transcurrent movements on any of the major cordilleran faults.

Transcurrent faults

The major transcurrent faults of the Canadian cordillera are shown in Fig. 2. The Denali, Queen Charlotte and Yalakom-Pasayten fault systems are too far west to accommodate movement of any elements of Terrane I. The Finlay fault system (Kutcho-Kechika-Finlay-Pinchi faults) has a total offset of ~300 km[18] and no true southern extension. The Fraser fault system can accommodate only ~150 km of early Tertiary move-